AD-A077 870 AERODYNE RESEARCH INC BEDFORD MA F/G 4/1
NITRIC OXIDE ION AND URANIUM OXIDE ION STUDIES.(U)
JUN 79 F BIEN F19628-76-C-0178
UNCLASSIFIED ARI-RR-171 AFGL-TR-79-0164 NL

| OF |
AD
A077870

END
DATE
FILMED
1-80
DDC

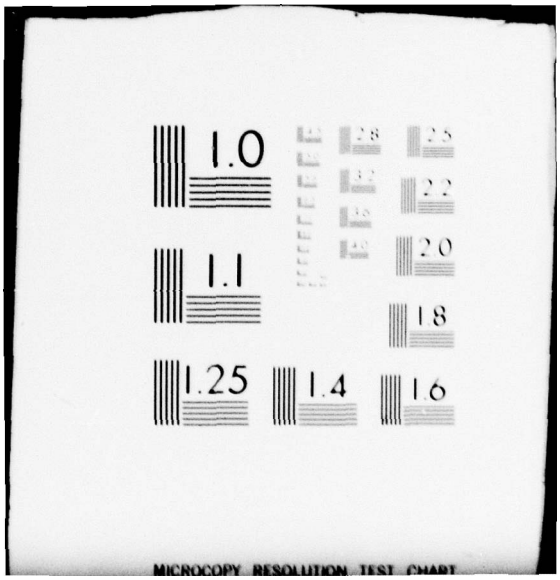
1.0
1.1
1.25
1.4
1.6
2.0
2.2
2.5
1.8
MICROCOPY RESOLUTION TEST CHART

AFGL-TR-79-0164

NITRIC OXIDE ION AND URANIUM OXIDE ION STUDIES

Fritz Bien

Aerodyne Research, Inc.
Bedford Research Park
Crosby Drive
Bedford, Massachusetts 01730

Final Report
25 March 1976 - 31 March 1979

June 1979

This research sponsored by the Defense Nuclear Agency, under Subtask S99QAXH1002, Work Unit 44, entitled, "Atomic and Molecular Physics of IR Emissions."

AIR FORCE GEOPHYSICS LABORATORY
AIR FORCE SYSTEMS COMMAND
UNITED STATES AIR FORCE
HANSCOM AFB, MASSACHUSETTS 01731

UNCLASSIFIED

SECURITY CLASSIFICATION OF THIS PAGE (When Data Entered)

REPORT DOCUMENTATION PAGE	READ INSTRUCTIONS BEFORE COMPLETING FORM
1. REPORT NUMBER: AFGL-TR-79-0164	2. GOVT ACCESSION NO. / 3. RECIPIENT'S CATALOG NUMBER
4. TITLE (and Subtitle): NITRIC OXIDE ION AND URANIUM OXIDE ION STUDIES	5. TYPE OF REPORT & PERIOD COVERED: Final Report - 3/25/76 - 3/31/79
	6. PERFORMING ORG. REPORT NUMBER: ARI-RR-171
7. AUTHOR(s): F. Bien	8. CONTRACT OR GRANT NUMBER(s): F19628-76-C-0178
9. PERFORMING ORGANIZATION NAME AND ADDRESS: AERODYNE RESEARCH, INC. Bedford Research Park, Crosby Drive Bedford, MA 01730	10. PROGRAM ELEMENT, PROJECT, TASK AREA & WORK UNIT NUMBERS: DDNA 0027
11. CONTROLLING OFFICE NAME AND ADDRESS: Air Force Geophysics Laboratory Hanscom AFB, Massachusetts 01731 Monitor/Robert E. Huffman/LKO	12. REPORT DATE: Jun 79 / 13. NUMBER OF PAGES: 39
14. MONITORING AGENCY NAME & ADDRESS (if different from Controlling Office): Final rept. 25 Mar 76-31 Mar 79	15. SECURITY CLASS. (of this report): Unclassified / 15a. DECLASSIFICATION/DOWNGRADING SCHEDULE: U

16. DISTRIBUTION STATEMENT (of this Report)

Approved for public release; distribution unlimited

17. DISTRIBUTION STATEMENT (of the abstract entered in Block 20, if different from Report)

I002

18. SUPPLEMENTARY NOTES

This research sponsored by the Defense Nuclear Agency, under Subtask S99QAXH1002, Work Unit 44, entitled, "Atomic and Molecular Physics of IR Emissions."

19. KEY WORDS (Continue on reverse side if necessary and identify by block number)

NO^+ f-numbers
UO^+ vibrational quenching
UO absorption coefficients

20. ABSTRACT (Continue on reverse side if necessary and identify by block number)

Spectroscopy of NO^+ and UO^+ are being studied. Apparatus for creating and measuring the radiative lifetime and spectral location of NO^+ vibration have been completed and are described.

The NO^+ (v) absorption coefficient and quenching of NO^+ (v) in the v = 1 and 2 states by N_2 have been experimentally determined. Integrated absorption coefficients corrected for a thermal equilibrium distribution are $S_{lu}(1-2\ P5) = 430\ cm^{-2}\ atm^{-1}$ and $S_{lu}(2-3\ R2) = 653\ cm^{-2}\ atm^{-1}$. Quenching of NO^+ (v) by N_2 at 297°K was found to

DD FORM 1 JAN 73 1473 EDITION OF 1 NOV 65 IS OBSOLETE S/N 0102-LF-014-6601

UNCLASSIFIED

SECURITY CLASSIFICATION OF THIS PAGE (When Data Entered)

390 112

Abstract (Cont.)

give rates of $k = 2.5 \times 10^{-12}$ cm^3 sec^{-1} for $NO^+(v=2)$ and $k = 3.0 \times 10^{-12}$ cm^3 sec^{-1} for $NO^+(v=1)$. An estimate of 3×10^{-13} cm^3 sec^{-1} was found for quenching of $NO^+(v=2)$ by NO at 297°K.

TABLE OF CONTENTS

APPENDIX

MEASUREMENTS OF THE NITRIC OXIDE ION VIBRATIONAL ABSORPTION COEFFICIENT AND VIBRATIONAL TRANSFER TO N_2

J. Chem. Phys., 69, 2631-38 (1978)

1. INTRODUCTION

The radiative lifetimes of infrared active ions are of particular importance in determining the background radiation in a disturbed atmosphere. The geomagnetic field striates ionic species causing these radiators to form a non-uniform background. Thus, even at lower concentrations than molecular species, ions play a more important role in the analysis of disturbed atmospheric signatures. This research was undertaken to measure the radiative lifetime and quenching of vibrationally hot ions NO^+ and UO^+. These molecular ions are of particular importance because of their low ionization energies. Nitric oxide has the lowest ionization energy for those ions that can be formed from the natural atmospheric species, N_2, O_2, and O. The disappearance of NO^+ in the upper atmosphere is dependent only on its dissociative recombination rate. The uranium oxide ion is endothermic to dissociative recombination, thus it is one of the most important metallic oxide ions in the upper atmosphere. Since its disappearance depends on three body recombination, this ion would be an important contributor to the 11-14 micrometers infrared signature in a disturbed atmosphere.

The measurement of the radiative lifetime and transfer rate of vibrational energy from NO^+ to N_2 has been measured and is presennted in the Appendix. The apparatus has since been modified to study the radiative lifetime of UO^+. Work directed toward the measurement of UO^+ radiation is presented in the following sections.

2. URANIUM OXIDE ION STUDIES

The prime importance of UO^+ in the upper atmosphere is that while relatively only small amounts of uranium are released into the atmosphere during a nuclear event, because of its ionic nature, it striates in the earth's geomagnetic field. Emission from this ion, primarily in the 12-14 μm atmospheric window,[1,2] is of major importance in understanding infrared backgrounds which would affect optical sensor systems designed to operate in this environment.

Uranium oxide ions formed in the upper atmosphere are stable to two body collisions. Because of their low ionization energies and the larger bonding energies for UO and UO_2, the formation of the oxide ions is exothermic. Dissociative recombination of these ions is in turn endothermic, and they require three body reactions to neutralize their charge. The lifetimes of these ions are thus expected to be very long compared to other ions created by a nuclear event. Because of this possibly very important source of infrared emission, the infrared spectra and radiative lifetime of this species must be known in order to predict the overall emission signature in the longwave infrared.

The spectra from vibrationally excited UO and UO_2 have been observed in matrix isolation studies carried out at NBS.[2,3] The emission from UO^+, however, has not been observed.[2,3] Because of the manner in which the vibrational spectra from UO and UO_2 were observed, the precise rotational spacing and anharmonicity constants have not been measured. With this scant amount

---

1. S. D. Gabelnick, G.T. Reedy, and M.G. Chasanov, "Infrared Spectra of Matrix Isolated Uranium Oxide Species In the Stretching Region," J. Chem. Phys., 58, 4468-75 (1973).

2. S. D. Gabelnick, G.T. Reedy, and M.G. Chasanov, "The Infrared Spectrum of Matrix Ioslated Uranium Oxide Vapor Species," Chem. Phys. Lett., 19, 90 (1973).

3. S.D. Gabelnick and G.T. Reedy, "Fine Definition of IR Spectra from High Temperature Interactions of $U+O_2$," DNA 3410F (1974) Prepared for Defense Nuclear Agency, Washington, D.C.

of information present, both the spectra and radiative lifetime of UO^+ are unknown. With the lack of knowledge of the molecular constants for UO^+, theoretical investigations such as those using configuration interaction techniques are good to within an order of magnitude at best.[4]

The next portion of the report describes the experimental technique and apparatus designed to measure the spectral location and radiative band strength of UO^+.

---

4. H.H. Michels , "Theoretical Determination of Metal Oxide f-Numbers," AFWL TR74-239 (1974) Prepared for Defense Nuclear Agency, Washington, D.C.

3. FORMATION OF UO AND UO^+

The thermal chemistry and infrared radiation of the uranium-oxygen system has been studied by several authors.[5-8] The reactions of importance are listed in Table 1. Using a triple crossed beam technique, Fite, et al. have shown that both Reactions 1 and 2 are gas kinetic, being 2.7 and 2.1 eV exothermic, respectively. The ionization potential for UO^+ is on the order of 5 eV, making it stable to dissociative recombination, thus, requiring three body recombination to return to the neutral species via Reactions 5 and 6.

Table 1. Reactions

REACTION	RATE	EXOTHERMICITY (eV)
R1 $U + O_2 \rightarrow UO + O$	$k = 4 \times 10^{-10}$ cm^3 sec^{-1} (5)	2.7 (5)
R2 $U + O \rightarrow UO^+ + e$	$k = 4 \times 10^{-10}$ cm^3 sec^{-1} (6)	2.1 (6)
R3 $U + O_2 \rightarrow UO_2^+ + e$	$k = 4 \times 10^{-12}$ cm^3 sec^{-1} (8)	4.1 (6)
R4 $U^+ + O_2 \rightarrow UO^+ + O$	$k = 8.5 \times 10^{-10}$ cm^3 sec^{-1} (8)	3.3
R5 $UO^+ + e + M \rightarrow UO + M$	$k = 10^{-26}$ cm^3 sec^{-1}	4.8
R6 $UO + O_2 \rightarrow UO_2 + O$		
R7 $UO^+ + O_2 \rightarrow UO_2^+ + O$	$k = 2 \times 10^{-9}$ cm^3 cm^{-1}	2

5. W.L. Fite, H.H. Lo, and P. Irving, "Associative Ionization in U+O and $U+O_2$ Collisions, J. Chem. Phys., 60, 1236 (1974).

6. W.L. Fite, T.A. Patterson, and M.W. Siegel, "Cross-Sections for Thermal Reactions Between Uranium Atoms and Atmospheric Species," AFGL TR77-0029, (1977).

7. W.L. Fite, and Hsi Hu Lo, "Reactions of UO^+ with Atmospheric Gases," AFGL TR 77-0029 (1977).

8. R. Johnsen and Manfred A. Biondi, "Reaction Rates of Uranium Ions and Atoms with O_2 and N_2," J. Chem. Phys., 57, 1975 (1972).

Since the atomic ground states for the formation of UO^+ are $U(^5L)$ and $O(^3P)$, there are 81 electronic states of UO which can dissociate to U and O. At least half of these would cross the ground state curve of UO^+ at an energy less than the dissociation energy, in which the curve crossing might lead to an UO^+ which is vibrationally excited. The ground state atomic ion $U^+(^4I)$ combined with $O(^3P)$ forms 63 electronic states of UO^+. A good portion of these states lie sufficiently low in energy to be formed by associative ionization of U + O.[5] These electronic states all have individual vibrational spectra. It is thus expected that the UO^+ vibrational spectra may have a very large line density; and individual vibration rotation spectra may not be separable. In this case, however, the gf values for the emission spectrum becomes very important for the prediction of UO^+ spectra in the atmosphere.

4. UO^+ ABSORPTION COEFFICIENT

The emission spectra of UO^+ is related to its absorption spectra by the ratio of the degeneracies of the upper to lower levels. It is easier to measure the absorption of light by these molecules than to measure their emission, however, because blackbody radiation from the apparatus is near a maximum at the wavelengths of interest.

The absorption coefficient for UO^+ vibration is a function of the extinction along the line-of-sight, given by Beer's law:

$$I(\lambda) = I_o(\lambda) \exp\left[(n_u - n_\ell)\sigma\ell\right] , \qquad (1)$$

where $I_o(\lambda)$ is the intensity of incident light at the wavelength λ, n_u and n_ℓ are the number densities of UO^+ in the upper and lower levels, respectively, σ the absorption cross-section, and ℓ the absorption path. The absorption path ℓ is given by the number of passes through the gas of interest times the pathlength through this gas. The intensity ratio $(I_o-I)/I_o$ is measured by tuning the laser through wavelength λ. The transmission through the test section with no absorption would give $I_o(\lambda)$. When the absorbing gas is put into the test section, the signal would drop to $I(\lambda)$. However, $I_o(\lambda)$ is a function only of the laser tuning and is relatively constant over the width of an absorbing line. Thus, in scanning the laser across the absorbing UO^+ line, part of the signal is absorbed out. The ratio to when no gas is in the test section is thus;

$$\frac{I_o - I}{I_o} \cong (n_\ell - n_u)\sigma\ell \qquad (2)$$

The number density n_u and n_ℓ are given by the product of their electronic, vibration and rotation partition functions times the total number density of UO^+. The rotational partition function for a molecule in the J^{th} rotation level is given by:

$$\phi_J = n_J/n = (2J + 1) \frac{hc\, B_v}{kT} \exp \left[-J\,(J+1)\, hc\, B_v/kT \right] \qquad (3)$$

where hc/k is the second radiation constant, T the temperature, B_v the rotational constant, and J the rotational level. The partitioning into vibrational level if vibrational equilibration occurs before the metallic ion is studied, is given by the Boltzmann factor:

$$\phi_{v_i} = \frac{\exp - \epsilon_i/kT}{\sum_i \exp (- \epsilon_i/kT)} \qquad (4)$$

where ϵ_i is the vibrational energy in the i^{th} vibrational level.

Since the flow time does not ensure vibrational equilibrium, several lines belonging to separate vibrational levels must be measured and their relative intensities must be measured as a function of quenching time, hence, the residence time before reaching the test section. This measurement gives both the vibrational relaxation rate of the infrared active species and the relative vibrational distribution produced by the $U + O_2$ reaction.

Assuming that the UO^+ is thermally equilibrated, the final temperature in a UO^+ argon mix would be 600^oK. Thus, approximately 0.86, 0.13, 0.017, 0.002 of all the UO^+ ions are in the v = 0, 1, 2, and 3 levels, respectively.

The assumption of rotational equilibrium is a better one. Since the rotational constant for UO^+ is expected to be about 0.3 cm^{-1}, the maximum concentration of UO^+ should be in the j = 26 rotational level. Approximately 2% of all UO^+ formed would be in this rotational level.

The electronic partition function presents more of a problem. Because of the large multitude of electronic states that would have energies low enough to be acceptable in the UO^+ formation, the partitioning into each of the various states must be measured using high resolution spectroscopy. In a worst case, emission spectroscopy may yield a large emitting quasicontinuum. This emission would impact what is expected in the upper atmosphere only if the same partitioning of electron energy is present there as in the laboratory.

The spectral absorption cross-section σ is determined once the total number density n is known, as well as the partition into the electronic, vibration and rotation states. This cross-section should vary with wavelength when a light source is tuned through an absorbing line. The spectral absorption cross-section, σ , for a molecule is a function of its integrated line absorption cross-section and its line width. At low pressures and high temperatures, the line width is given by the Doppler profile, the Doppler full width half maximum is:

$$b_D = \left(\frac{8\ kT\ \ln 2}{m\ c^2} \right) \omega_{lu} \tag{5}$$

where m is the mass of the molecule, and ω_{lu} is the wavenumber of the particular transition. At line center, assuming a Doppler line shape, the absorption cross-section is:

$$\sigma(0) = S_{lu} \left(\frac{m\ c^2}{2\pi\ kT} \right)^{\frac{1}{2}} \frac{1}{\omega_{ul}} \tag{6}$$

where S_{lu} is the integrated absorption coefficient per molecule and σ (0) is the spectral absorption cross-section at line center. The line center is conveniently found by using derivative spectroscopy. By fine tuning the laser light across the line center, the absorption goes through a maximum, hence, the output through the gas goes through an intensity minimum. Thus, by putting an a.c. component onto the tuning of the laser, and looking at the rate of change in the intensity signal, this rate crosses zero at the line center.

Again, in thermal equilibrium, this S is related to the Einstein A coefficient by:

$$S_{lu} = \frac{A_{ul}}{8\pi\omega_{lu}^2\ c} \frac{g_u}{g_l} \left(1 - \exp \frac{hc\ \omega_{lu}}{kT} \right) \tag{7}$$

where g_u and g_l are the statistical weights of the upper and lower states, respectively, and A_{ul} in units of sec^{-1}, is the Einstein A coefficient for the transition of wavenumber ω_{lu}, in units of cm^{-1}, and S_{lu} has units of $cm^2 - cm^{-1}$. Thus, for a 1 sec lifetime, $A_{ul} = 1\ sec^{-1}$, and $S_{lu} = 3 \times 10^{-18}$ cm. The spectral line absorption cross section at $600^{\circ}K$ on line center is thus $\sigma = 2 \times 10^{-16}\ cm^2$ at line center. This cross section would cause a 1/e extinction for a concentration of $4 \times 10^{14}\ UO^+$ per cm^3 in the present experimental apparatus.

5. EXPERIMENTAL ARRANGEMENT

The experimental arrangement for the measurement of the spectral location and line intensity of UO^+ consists of several separate portions. A schematic diagram of the apparatus is shown in Figure 1. Separate descriptions of the flow system, the evaporation system and the optical train are described below.

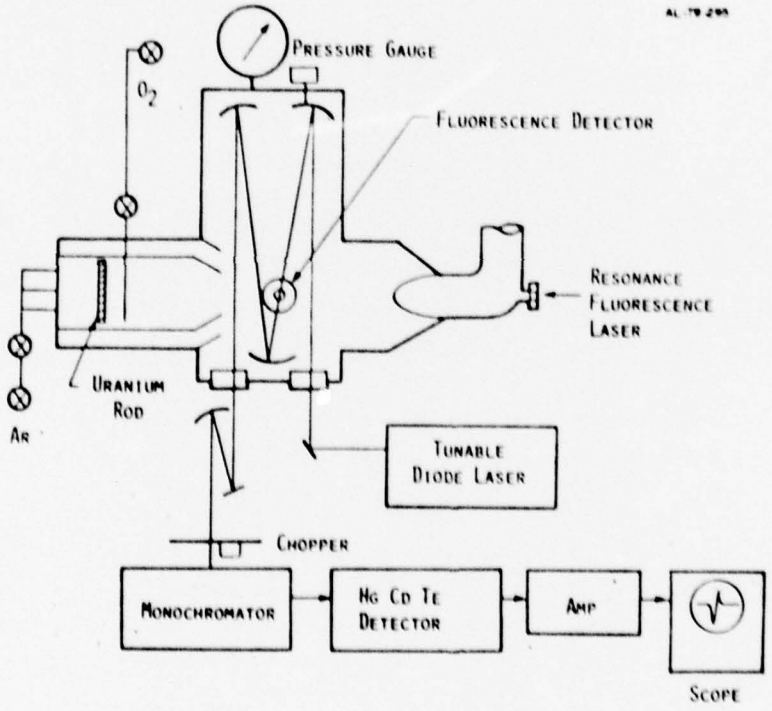

Figure 1. Schematic Diagram of Uranium Oxide Ion Absorption Measuring Apparatus.

5.1 Flow System

The flow system is designed to mix uranium metal vapor with molecular oxygen to form uranium oxide. The excess uranium vapor then mixes with the atomic oxygen liberated from the first reaction to form uranium oxide ion. Because of its very good wetting characteristics, the uranium must be kept from the side walls before mixing with the oxygen. This is done by using an Argon carrier gas to carry the uranium down the channel into the oxygen jets.

A schematic of the flow system is shown in Figure 2. Argon carrier gas carries the uranium vapor forward until it mixes with a jet of oxygen. The uranium vapor reacts gas kinetically with molecular oxygen as given in Reaction 1. The atomic oxygen liberated by this reaction goes to form UO^+ via Reaction 2. By changing the oxygen flow rate, the mixing ratios of UO to UO^+ can be varied. Depending on the O_2 flow rate, UO_2 and UO_2^+ can also be formed.

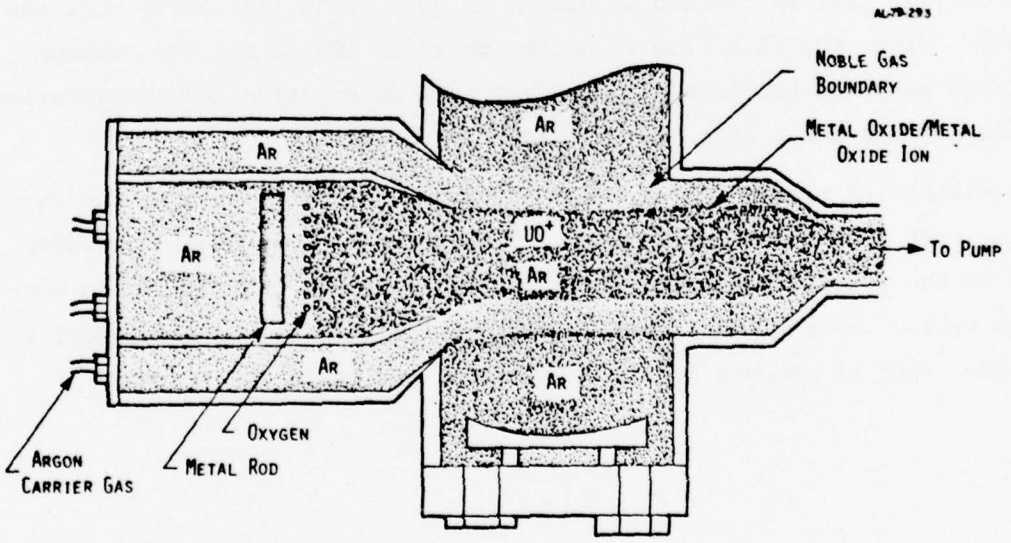

Figure 2. Diagram of Flow System for UO^+ Formation.

The uranium oxide and oxide ion are confined to the test section of interest by a containing flow of Argon. This external channel forms an aerodynamic window to prevent uranium oxide from depositing on the optics used in the UO^+ measurement. The flow rate of the shroud flow is adjusted such that its velocity matches that of the inner core flow. By operating at 10 torr or less pressure, the core flow, thus confined, provides an absorption path of 10 cm through the test region.

The flow velocity is measured by the pressure and flowrate. This velocity is governed by the flow of carrier gas, Ar, through the system. The primary importance of the gas velocity is in determining the degree of the reaction. This is only of a secondary importance in the measurement when the measurement is carried out sufficiently far downstream.

The carrier gas, introduced at $300^{o}K$, is used to collisionally cool the UO^+ formed. Since the flow time is on the order of 10-100 ms, the uranium oxide formed would be collisionally cooled, both in rotation and in vibration, to a mixture temperature near that of the carrier gas.

The mixture of uranium oxide vapor and Argon gas is trapped on the far end of the test section by a cold trap. Because of the extremely low vapor pressure of the refractory oxide, it is easily condensed when coming in contact with walls. By passing through a circulation path of the cold trap, the metal oxide vapor is removed before the carrier gas reaches the pumps.

5.2 Uranium Source

The source of uranium vapor is a depleted uranium rod which is evaporated by an electron beam. The electron beam is generated by a 30 kV, 300 ma Pierce-type electron gun originally designed for electron beam welding as shown in Figure 3. This gun was modified so that it could be differentially pumped to provide sufficient vacuum for electron beam operation as well as allowing high pressure operation (4 torr) of the uranium oxide flow tube source.

The Pierce-type electron gun consists of a cathode heated by a large current supply which in turn floats on a high voltage. The cathode filament, made of tantalum, is thus operated to as high as 300 ma and 30 kV. The cathode to grid voltage is provided by a set of dry batteries, wired in 510 volt increments. This grid supply provides the voltage to current characteristics for the electron gun. The actual operating power of the electron beam is then varied by changing the cathode voltage to the anode ground.

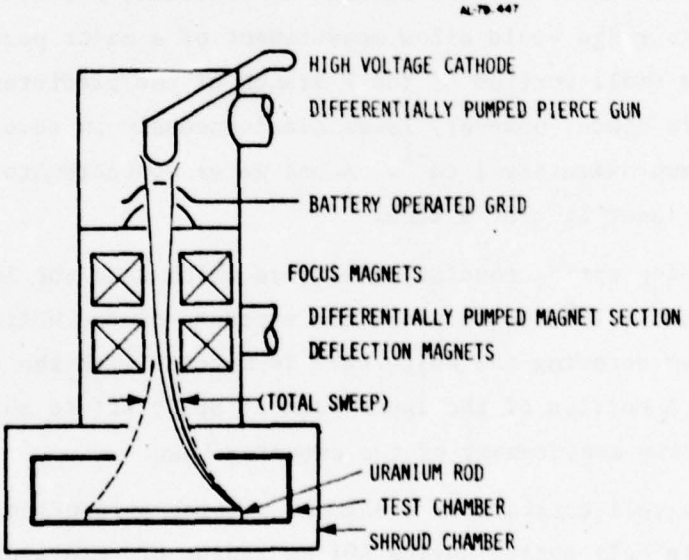

Figure 3. Electron Gun Evaporation Scheme.

The evaporation of the uranium is in the form of a virtual line source as the deflection magnets are operated in an a.c. fashion. The sweep speed is adjusted such that sufficient evaporation is achieved without undue losses in thermal heating of the uranium rod. Because of some stray inductance, the sweep of the electron beam across the uranium rod is not quite linear. This is not a real problem except it must be accounted for in the design of the differential pumping ports. The flow system, described above, carries the uranium vapor downstream from the rod, forming almost a continuous flow source.

5.3 Optical Train

The optical train to measure UO^+ absorption consists of a tunable diode laser, laser beam shaping optics, a multi-path absorption cell (White cell), a monochromator and an HgCdTe detector (see Figure 1). In addition to this optical train, is a second optical train at right angles, consisting of a visible dye laser, beam shaping optics, a photomultiplier, and gating electronics.

The tunable diode laser is tunable continuously between 800 and 862 cm^{-1}. This range would allow measurement of a major portion of the P branch and a small portion of the R branch of the predicted UO^+ vibrational spectrum. This diode, however, lases simultaneously in several laser lines, separated by approximately 1 cm^{-1}. A one meter monochromator is thus used to select one laser line at a time.

Beam shaping optics consist of mirrors which take the laser beam, diverging at 60° x 15°, to focus on the entrance of the White cell. The converging beam entering the White cell is matched with the f:18 of the White cell optics. A portion of the laser beam is split off to obtain an instantaneous intensity measurement of the entering beam.

The White cell consists of a chamber running perpendicular to the flow tube with White cell optics having 401 mm radius of curavature. Two spherical mirrors 50 mm in diameter are used. The field mirror is split in the middle, forming two halves, 25 mm by 50 mm. Two slots are cut into the front mirror to allow entrance and exit of the laser beam. The White cell mirrors

are gold coated to maximize reflectivity in the 11 μm region. Mirror losses become important when many traversals are made through the test region. When the fractional light loss due to one reflection becomes larger than the extinction of light from an extra pass through the test region, more passes in the White cell would not increase the signal-to-noise ratio. For very small absorption coefficients, this White cell is practically limited to 68 passes, equal to a 1/e drop in the laser intensity due to mirror losses alone.

The laser beam, after traversing the White cell 68 times, exits and is again brought to focus, this time to match the f:10 optics of a 1m McPherson Czerny-Turner monochromator. The output of the monochromator is brought onto the surface of an 3 mm square HgCdTe detector, whose signal is fed into either an oscilloscope or a lock-in amplifier. The wavelength tuning of the tunable diode laser across the width of the monochromator spectral width is also fed into the lock-in amplifier. This phase locked system measures the absorption of light at any particular phase as the laser is tuned across the absorbing line.

By taking the change slope of the absorption line, both the line intensity and location can be deduced, provided the shape of the line is known. This second derivative measurement of the absorption is several orders of magnitude more sensitive than measurement of extinction alone because it is unnecessary to establish a firm baseline using this technique.

Perpendicular to the White cell optics in the absorption cell, is placed the focus of a tunable dye laser, tuned to the uranium resonance line at 358.5 nm. Since the gf value has been measured for this line, resonance fluorescence at this wavelength gives a measure of the uranium concentration formed by the electron gun evaporation technique. Perpendicular to both the dye laser and the White cell is placed a 1P28 photomultiplier to detect this fluorescent signal. The uranium concentration can thus be monitored with and without oxygen to form UO and UO^+.

6. TESTING AND CALIBRATION

In order to measure the radiative lifetime and spectral location of UO^+, steps must be taken to insure the safety of the personnel involved in the experiment. Even though the total concentration of uranium vapor is very low, depending on the radiative lifetime and operating time, a large amount of uranium vapor may be deposited on the inside walls of the experimental apparatus. The pyrophoric nature of uranium vapor requires some specialized handling techniques for the disassembly and cleaning of the apparatus. Standard safety procedures have been devised to this end.

Since there is some uncertainty as to what would be the total amount of uranium vapor made before the experiment becomes operational, it is desirable to use other metal oxide species to characterize and calibrate the apparatus before introducing uranium into the system. The testing of the electron beam and flow system could thus be performed without the risk of heavy metal contamination.

The electron beam evaporation system has been tested using the electron gun to evaporate aluminum as well as carbon. While aluminum has a much higher vapor pressure than does uranium, its much higher thermal conductivity makes it a fair simulation for determining the ultimate uranium yield using this system. Electron beam evaporation of a graphite rod has the opposite thermal dependence. The carbon vapor pressure is very low, however, the thermal conductivity of carbon is also very low. The additional problem of carbon sputtering was also encountered. Blackbody temperatures of the order of $2500^{\circ}K$ measured by an optical pyrometer was obtained using both the aluminum and carbon sources. This temperature proved to be a lower limit to the evaporation temperature, as the electron beam quickly etched a channel into the material being evaporated. Since only the temperature of the surface within the field-of-view could be measured using this technique, measurements could only be taken before much material had been evaporated.

The vapor pressure of the carbon source was measured by measuring the pressure rise through the flow system when the electron beam was operated. This measurement showed that a 1 torr pressure of carbon vapor could be maintained even at maximum pumping speed, which provided a flow velocity on the order of 100 m/sec through the 2 x 10 cm channel. The electron beam energy required to maintain this vapor pressure was 12 kV at 35 ma. Higher electron beam powers were available. However, the vapor pressures above about 10 torr would cause the differentially pumped electron gun chamber to rise to unacceptable pressure ($p > 10^{-3}$ torr).

The flow system, consisting of an inner core flow, in which the metal oxide of interest is contained and an outer shroud flow was studied in a Reynolds number matching simulation using water with chemiluminescent dye for flow visualization. These tests provided the operating parameters for the actual gas handling system. Actual flow visualization, using a metal oxide vapor, has not been carried out in the apparatus.

7. CONCLUSIONS

The final status of the experiment to measure the spectral characteristics of UO^+ is as follows: The apparatus designed to produce UO^+ has been constructed. Diagnostics have been designed and constructed to independently monitor the UO^+ production. Diagnostics have been constructed to monitor the uranium atom production. The optical train has been constructed and aligned to measure the spectral absorption of UO^+ in the 11 to 14 μm region. A diode laser has been calibrated and aligned to measure the UO^+ absorption between 790 and 820 cm^{-1} (12.2 to 12.6 μm).

It was not possible to carry out any actual experimental measurements, however, because of lack of resources and time. This extra requirement for time and resources was brought about by the unanticipated additional effort required for the handling of uranium. Even though a very depleted uranium is being used, the possibility of heavy metal poisoning, as well as the low level alpha particle emission by uranium, required revisions in the apparatus which were designed originally for the study of safer ions. Special handling procedures, some of which have not been completed as yet, are being devised for this experiment.

The apparent toxicity of uranium is compounded by its pyrophoric nature. Unoxidized uranium on the walls of the apparatus quickly oxidizes and leaves in an oxide vapor when the apparatus is exposed to the atmosphere. The disposal of uranium and uranium oxides after passing through the apparatus was addressed too late in the program to allow any meaningful measurements on UO^+. Cold traps and valves have since been designed to allow disassembly and cleaning of apparatus of uranium and disposal of the uranium. Construction of these portions of the apparatus, however, has not been completed.

In order to optimize the probability of success in measuring the UO^+ spectral absorption coefficient, it is desirable to use the same technique on

other, less toxic, metal oxides and metal oxide ions first. Other metal oxides which radiate in the 10 to 14 μm region and are of possible interest in a disturbed atmosphere are AℓO and FeO. While these oxides are much less toxic than UO^+, the measurement technique to determine their radiative lifetimes are essentially the same as that for UO^+.

8. REFERENCES

1. S. D. Gabelnick, G.T. Reedy, and M.G. Chasanov, "Infrared Spectra of Matrix Isolated Uranium Oxide Species In the Stretching Region," J. Chem. Phys., 58, 4468-75 (1973).

2. S. D. Gabelnick, G.T. Reedy, and M.G. Chasanov, "The Infrared Spectrum of Matrix Ioslated Uranium Oxide Vapor Species," Chem. Phys. Lett., 19, 90 (1973).

3. S.D. Gabelnick and G.T. Reedy, "Fine Definition of IR Spectra from High Temperature Interactions of $U+O_2$," DNA 3410F (1974) Prepared for Defense Nuclear Agency, Washington, D.C.

4. H.H. Michels , "Theoretical Determination of Metal Oxide f-Numbers," AFWL TR74-239 (1974) Prepared for Defense Nuclear Agency, Washington, D.C.

5. W.L. Fite, H.H. Lo, and P. Irving, "Associative Ionization in U+O and $U+O_2$ Collisions, J. Chem. Phys., 60, 1236 (1974).

6. W.L. Fite, T.A. Patterson, and M.W. Siegel, "Cross-Sections for Thermal Reactions Between Uranium Atoms and Atmospheric Species," AFGL TR77-0029, (1977).

7. W.L. Fite, and Hsi Hu Lo, "Reactions of UO^+ with Atmospheric Gases," AFGL TR 77-0029 (1977).

8. R. Johnsen and Manfred A. Biondi, "Reaction Rates of Uranium Ions and Atoms with O_2 and N_2," J. Chem. Phys., 57, 1975 (1972).

APPENDIX

MEASUREMENTS OF THE NITRIC OXIDE ION VIBRATIONAL ABSORPTION COEFFICIENT AND VIBRATIONAL TRANSFER TO N_2

J. Chem. Phys., 69, 2631-38 (1978)

Measurements of the nitric oxide ion vibrational absorption coefficient and vibrational transfer to N_2 [a)]

Fritz Bien

Aerodyne Research, Inc., Bedford, Massachusetts 01730
(Received 2 September 1977)

The $NO^+(v)$ absorption coefficient and quenching of NO^+ vibration in the $v = 1$ and $v = 2$ states by N_2 have been experimentally determined. Integrated absorption coefficients corrected for a thermal equilibrium distribution are: $S_{1_w}(1\text{–}2\ P\ 5) = 430\ cm^{-2}atm^{-1}$ and $S_{1_w}(2\text{–}3\ R\ 2) = 653\ cm^{-2}atm^{-1}$. Quenching of $NO^+(v)$ by N_2 at 297°K was found to give rates of $k = 2.5 \times 10^{-12}\ cm^3sec^{-1}$ for $NO^+(v = 2)$ and $k = 3.0 \times 10^{-12}\ cm^3sec^{-1}$ for $NO^+(v = 1)$. An estimate of $3 \times 10^{-13}\ cm^3sec^{-1}$ was found for quenching of $NO^+(v = 2)$ by NO at 297°K.

I. INTRODUCTION

Interest in NO^+ vibrational band intensities stem from its relatively large population in electron disturbed atmospheres. The nitric oxide ion is the most abundant ion in auroral and other electron excited events. The principal source of NO^+ in the upper atmosphere is from ion exchange reactions $N_2^+ + O \rightarrow NO^+ + N$ and $O^+ + N_2 \rightarrow NO^+ + N$ and the charge exchange reactions of N_2^+, N^+, O^+, and O_2^+ with natural atmospheric NO. Since all of these reactions are exothermic enough to excite several vibrational levels in NO^+, $NO^+(v)$ may provide an important source of infrared emission in the electron disturbed upper atmosphere.

Radiation from vibration of $NO^+(X^1\Sigma^+)$ is in the 4.3 μm band, coincident with the $CO_2(\nu_3)$ emission. While $CO_2(\nu_3)$ emissions dominate in the undisturbed atmosphere, self-absorption by cold CO_2 limits its emission signal to the wings of the CO_2 band. Since many sensor systems are currently being designed to operate in these regions, the effects of $NO^+(v)$ radiation on these systems may be of great importance. Because of the intense $CO_2(\nu_3)$ emission, $NO^+(v)$ radiation has not been detected during auroral events except perhaps to explain very prompt emission during an IBC III aurora.[1,2] The only unambiguous NO^+ emission in the upper atmosphere was observed during a nuclear test in 1962.[3]

While the radiative lifetime of NO^+ has never been measured, Stair and Gauvin[3] have inferred an integrated absorption coefficient of $S_{1_w} = 500\ cm^{-2}atm^{-1}$ from the 1962 nuclear observations past the CO_2 blue spike region. This value was obtained through various assumptions of vibrational equilibrium and atmospheric transmission. The only other information of the vibrational lifetime of NO^+ has been from *ab initio* calculations by F. Billingsley[4] and H. H. Michels.[5] Billingsley obtained a ground state integrated absorption coefficient of $S_{1_w} = 88.9\ cm^{-2}atm^{-1}$ using a multiconfiguration self-consistent field (MCSCF) approach. Similarly, Michels arrived at a calculated value of $S_{1_w} = 168\ cm^{-2}atm^{-1}$.

The purpose of this study is to measure the radiative lifetime of NO^+ vibrational bands in the $X^1\Sigma^+$ ground state and to measure the transfer of vibration between NO^+ and N_2, whose vibrational energies are in close resonance.

This paper describes the experimental determination of NO^+ $\Delta v = 1$ integrated absorption coefficient in the $v = 0$, $v = 1$, and $v = 2$ levels and quenching of the $v = 1$, $v = 2$, and $v = 3$ levels by N_2. The experimental arrangement is presented in Sec. II. Results of the experimental determination of the NO^+ absorption coefficient are presented in Sec. III. In Sec. IV, we discuss the experimental determination of the quenching of $NO^+(v)$ by N_2. A discussion of our results is presented in Sec. V.

II. EXPERIMENTAL ARRANGEMENT

The experimental arrangement for measuring the absorption of NO^+ is shown in Fig. 1. Approximately 1 torr of research grade nitric oxide was put into the test chamber. The nitric oxide was photoionized by a set of

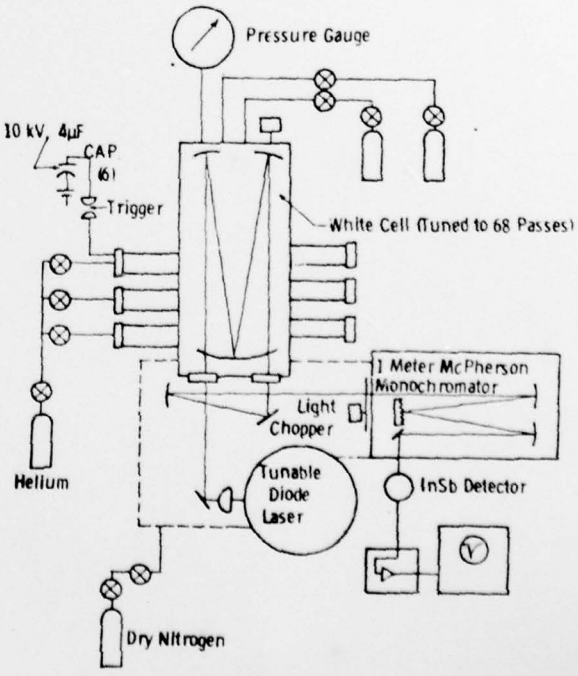

FIG. 1. Schematic diagram of the experimental arrangement.

a)This work was sponsored by Air Force Geophysics Laboratory (Air Force Systems Command) under Contract No. F19628-76-C-0178—funding was by the Defense Nuclear Agency.

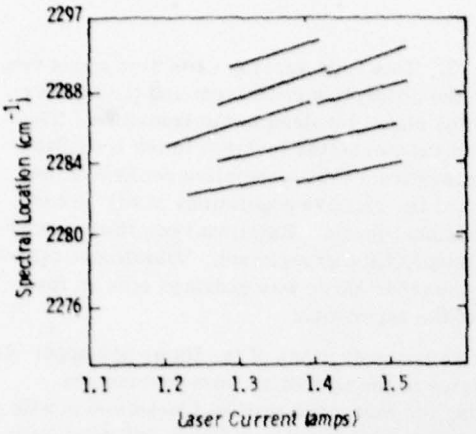

FIG. 2. Typical laser tuning curves from the diode laser. Relative laser intensities varied with time and laser current.

six ultraviolet discharge lamps, three on each side of the chamber. These flash lamps provided an active region approximately 15 cm long in which NO* was formed. The photoionized NO* was studied in absorption by passing a beam of infrared laser light through the photoionization region. *White cell optics*[6] were placed on the two ends of the chamber to allow multiple passes of the infrared laser light through the photoionized region. Light absorbed by NO* formed in this region, together with the number density of NO* in the chamber, gave the absorption coefficient for the particular vibration-rotation state of interest.

A tunable diode laser (Laser Analytics) was used for the infrared source to measure the NO*(v) absorption. This laser was brought to focus on the entrance aperture of the White cell optical arrangement. Up to 104 passes through the NO* region were obtainable using this arrangement. However, only 68 passes were used during experimental runs, maximizing the absorption while minimizing mirror reflectivity losses. The laser beam, after exiting from the White cell mirrors, was brought to focus on the entrance slit of a 1 m Czerny-Turner monochromator. The monochromator was used to both select the frequency mode of the laser and to filter out the infrared components of the uv lamp energy. To accomplish this, the slitwidth of the monochromator was set to give a spectral half-width of 1 cm^{-1} in the laser spectral region. The light exiting from the monochromator was brought to focus on a 1 mm diam. InSb photovoltaic detector whose signal was amplified and fed into an oscilloscope. Because of the spectral coincidence between NO* and CO_2 bands, the entire optical train was flushed with dry nitrogen. The spectral locations of specific CO_2 lines were also used for laser frequency calibration.

The reference transmission level through the optical train was obtained by chopping the optical path in front of the monochromator. This chopped signal gave the system transmission in the absence of NO*. The chopper was then turned off in the open position during the operation of the photoionizing lamps. The ratio of laser intensity transmitted after the formation of NO* to that before formation of NO* thus provided the spectral extinction rate which was both a function of the laser wavelength and time. Since the half-width of the laser line ($\sim 10^{-4}$ cm^{-1}) was much narrower than the Doppler width of the absorbing line ($\sim 5\times10^{-3}$ cm^{-1}), the integrated absorption coefficient of the NO*(v, J) transition could be measured by tuning the laser across several points of the absorption line.

A typical calibration curve for the tunable diode laser is shown in Fig. 2. Because of the temperature cycling of the diode from room temperature to 10°K as the laser Dewar was filled, the actual tuning range varied from day to day. However, the laser usually tuned over at least one vibration rotation line per temperature cycling. Note that the tuning slope of the laser varied with current. The actual tuning slope for the particular wavelength of interest was obtained for each run, in order to obtain the absorption half-width, as well as location of the absorbing NO*(v) line.

The ultraviolet lamps used in this apparatus were of a modified Lyman configuration providing a 29 000°K black-body continuum radiation when discharged.[7,8] Helium gas was flowed through the lamps at approximately 3 torr pressure. All six lamps were discharged simultaneously by triggering six spark gaps in parallel, each connecting one flash lamp to a high speed capacitor charged to 10 kV at 4 μF. The time synchronization between lamp discharges was within 1 and 2 μsec in all experimental runs.

The output from each lamp was monitored by an ionization detector placed behind the region monitored by the White cell optics in the absorption chamber. The purpose of these ion detectors was to ensure that sufficient ion pairs were produced during each experimental run. The actual ion density, as a function of time, was determined separately. Each ionization detector consisted of a pair of parallel plates across which was put a 300 V potential. Electrons produced in the photoionization would be attracted to the anode plate causing current to flow. The cathode and anode were shielded from uv light through a pair of guard rings placed at ground potential. The potential difference between the anode and ground was measured across a 330 Ω resistor. The change in potential was then proportional to the current through the anode, and hence, the number of photoelectrons produced. Using this measurement scheme, it was established that more than 10^{13} ions pairs per cm^3 were produced per flash along the lamp axis within the absorption cell when the cell was filled to 1 torr with NO.

In order to obtain the vibrational transfer cross section from NO*(v) to N_2, provision was also made to bleed a partial pressure of N_2 into the absorption chamber. The pressure in the cell was monitored by a baratron pressure gage, reading from 0 to 10 torr with a least count of one part in 10^4. The partial pressure of N_2 was raised until NO*(v) transfer to N_2 caused a more rapid decrease in the extinction of diode laser signal in the $v=1$ and higher vibrational states than would be attributable to dissociative recombination. The quenching of

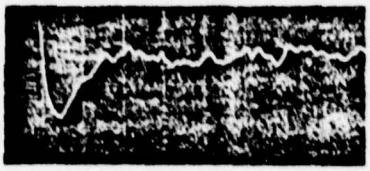

FIG. 3. Typical oscilloscope trace of the ac component of transmitted laser light. Horizontal scale represents 10 μsec/division, vertical 20 mV/division. The test chamber was filled with 1 torr of NO and 1 torr of N_2. The laser line was tuned to approximately the peak of the $NO^+ v = 2$ to $v = 3$, $R2$ absorption line.

laser light extinction by N_2, as a function of N_2 pressure, thus gave a transfer rate of $NO^+(v, J)$ to N_2.

The absorption of laser light by NO^+ formed during photoionization typically gave a signal as shown in Fig. 3. This trace represents the ac component of laser light falling on the detector. Discharge noise caused a large positive spike which triggered the oscilloscope. NO^+ formed by photoionization absorbed the laser emission giving the drop in total intensity. Dissociative recombination, together with quenching of the vibration rotation line by NO and, as in Fig. 3, 1 torr of N_2, caused the signal level to return to its dc level. The noise at late times was typical of the detector noise within the system even when no laser signal was present.

III. MEASUREMENT OF NO^+ ABSORPTION COEFFICIENT

The absorption coefficient for $\Delta v = 1$ vibrational transition in the $NO^+(X^1\Sigma^+)$ ground electronic level was obtained by measuring the time varying extinction described above. When the laser wavelength was coincident with the $NO^+(v)$ line, some extinction of laser radiation would result after the flash lamps were fired as seen in Fig. 3. This time varying extinction was a measure of both the absorption coefficient and the number densities of the states involved in the transition. The populations of the two states involved in the transition were determined from the dissociative recombination rate of NO^+ and the relative populations of NO^+ in the various vibrational levels. Rotational equilibrium was assumed throughout the experiment. Vibrational equilibrium, on the other hand, was assumed slow in the time scale of the experiment.

The relative concentrations of the lower and upper vibrational states in the transition were determined through fitting the measured window transmission with a predicted spectrum from the uv lamps and previously measured spectral data on photoionization.[9] Since MgF_2 windows were used in front of the uv lamps, the bandpass through which photoionization could occur was limited from 1130 to 1337 Å. Fortunately, there have been many studies in the threshold region of the NO photoionization.[9-11] From the measured photoionization efficiency in this region, the measured window transmission in this region, and assuming a lamp output of 30 000 °K black-body continuum, the relative photoionization was obtained as a function of wavelength. This is plotted in Fig. 4. Also plotted are the effects of uv lamp temperature of 40 000 and 20 000 °K black body. The vibrational partition, using this technique and the vibrational partitions measured as a function of uv wavelength by Tanaka *et al.*,[9] gave 0.29, 0.39, 0.22, 0.08, and 0.02 for the relative populations of the $v = 0$ through $v = 4$ levels, respectively.

The spectral absorption cross section for a molecule is given by Beer's law

$$\sigma = \frac{1}{Nl} \ln\left(\frac{I_0}{I}\right) , \tag{1}$$

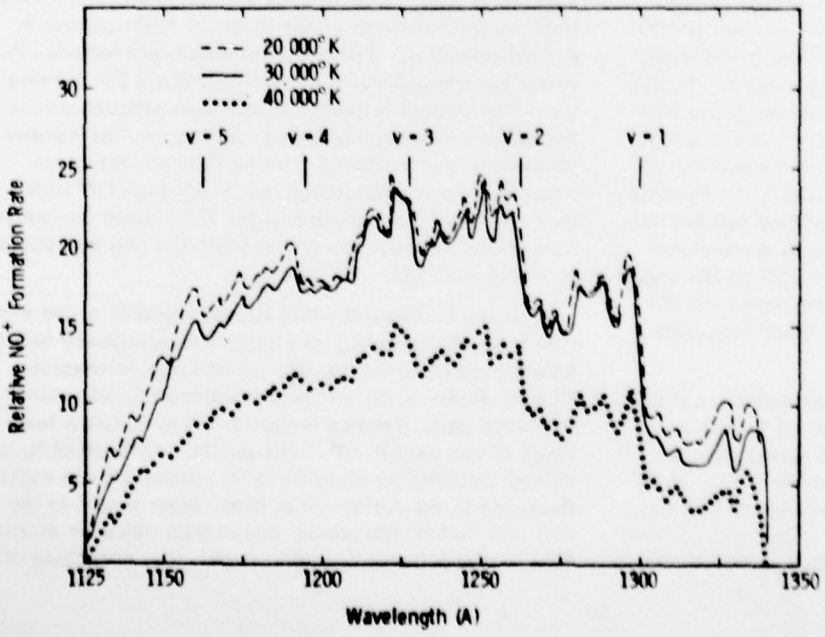

FIG. 4. Plot of NO photoionization efficiency through MgF_2 windows as a function of lamp output temperature. The threshold energy for exciting $v = 1$ thru 5 vibrational levels of NO^+ are shown. Relative $NO^+(v)$ concentrations obtained by folding this spectrum with vibrational partitions are given in Ref. 9.

TABLE I. $NO^*(v)$ rotation lines within laser bandpass.

Vibrational transition		Calculated location (cm^{-1})	Measured location (cm^{-1})	Cross section at peak (cm^{-1})
$v=0$ to 1	$P12$	2294.1		
	$P13$	2289.7	2289.76	$5\times10^{-16}(\pm2\times)$
	$P14$	2285.2		
	$P15$	2280.7		
$v=1$ to $v=2$	$P5$	2291.6	2291.63	$1.5\pm0.4\times10^{-15}$
	$P6$	2287.4	2287.45	$1.3\pm0.5\times10^{-15}$
	$P7$	2283.3	2283.35	
$v=2$ to $v=3$	$R1$	2282.8		
	$R2$	2286.7	2286.72	$2.2\pm0.3\times10^{-15}$
	$R3$	2290.4		
	$R4$	2294.4		
$v=3$ to $v=4$	$R10$	2282.7		
	$R11$	2286.1	2286.30	$2\pm1.5\times10^{-15}$
	$R12$	2289.5		
$v=4$ to $v=5$	$R20$	2281.9		
	$R21$	2284.9		
	$R22$	2287.8		

where N is the number of molecules in the absorbing level, and l is the total path length in the absorbing gas, equal in this case to the number of passes in the White cell times the length of the photoionized region. The quantities I and I_0 are the transmitted light intensities with and without absorption, respectively.

The concentration N is a function of the photoionization cross section, the recombination rate, and the relative number of molecules in the particular vibration-rotation level. Thus, N can be expressed as

$$N = \phi_R N_v(t) , \tag{2}$$

where ϕ_R is the rotation partition function and $N_v(t)$ is the number density in vibration level v. In this experiment, rotational equilibrium was assumed, as the rotational relaxation time was approximately an order of magnitude faster than the shortest experimental time of interest. Thus, the rotational partition function is

$$\phi_R = (2J+1)\frac{hcB}{kT}\exp\left[-J(J+1)\frac{hcB}{kT}\right] , \tag{3}$$

where J is the rotational level and B the rotational quantum number. The rate of change of the number density of NO^* in vibrational level v is given by

$$\frac{dN_v}{dt} = -\alpha_v N_v N_e - kN_v M^2 , \tag{4}$$

where α_v is the recombination rate of NO^* in vibrational level v, N_v the concentration of $NO^*(v)$, N_e the electron concentration, and k is the attachment coefficient of N_v to M. The initial condition to Eq. (4) is

$$N_{v_0} = \phi_v N_0 , \tag{5}$$

where ϕ_v is the relative production rate of NO^* in vibrational level v and N_0 is the total number density of NO^* produced. By operating at low enough NO pressures so that the second term on the right hand side of Eq. (4) may be neglected, and assuming α_v is relatively independent of v, the concentration of NO^* in the vibrational level v, and rotational level J, is

$$N = \phi_R\phi_v\frac{N_0}{1+N_0\alpha_v t} . \tag{6}$$

The total absorption by $NO^*(v, J)$, from Eq. (1), must be time dependent, such that $\ln(I_0/I)$ must vary as $1/N$. During the experiment, the ratio $(I_0 - I)/I_0$ was at all times less than 10^{-2}. Thus, $\ln(I_0/I)$ may be substituted by the expansion giving

$$\ln(I_0/I) \simeq (I_0 - I)/I_0 \equiv \Delta I/I_0 . \tag{7}$$

Note that the choice of $t=0$ in Eq. (6) can be rather arbitrary, provided that there is no production term in Eq. (4). Since both $\Delta I/I_0$ and $1/N$ must have the same time dependence, the concentration N at any time t_0 may be calculated by the relation

$$\frac{\Delta I(t_0)}{\Delta I(t_0+t)} = 1 + N(t_0)\alpha_v(t - t_0) . \tag{8}$$

Here, it may be seen that $N(t_0)$ is not a function of the total extinction but only of the rate of change of extinction with time. The number density can thus be related to the change in ac intensity with time. It is assumed here that no other quenching of $NO^*(v)$ is occurring simultaneously.

The tuning range of laser overlapped several vibrational rotation lines in NO^*. These lines are listed in Table I. While there were laser lines which overlapped all of the $NO^*(v)$ lines listed, measurements of the integrated absorption coefficient were made only of the $P5$ line of the $v=1$ to $v=2$ transition and the $R2$ line of the $v=2$ to $v=3$ transition. In addition, spectral absorption coefficients were obtained for the $R11$ line of the $v=3$ to $v=4$ transition and the $P13$ line of the $v=0$ to $v=1$ transition. Unfortunately, due to the low signal-to-noise ratio of these latter two measurements, sufficient data was not available to obtain a meaningful integrated absorption coefficient from these two transitions. Similarly, the $P6$ line of the $v=1$ to $v=2$ transition was measured using a rather weak laser line, which was near the mode shifting threshold of the laser. Because of the uncertainty introduced by the laser shift, the integrated absorption coefficient was not obtainable using this transition.

The locations of the lines of interest were found by measuring the locations of known CO_2 lines[12] and interpolating across the tuning range to obtain the precise location of the NO^*. In this way, the $P5$ line of NO^* ($v=1$ to $v=2$) was found to be at 2291.63 cm^{-1}, while $R2$ line of the $v=2$ to $v=3$ transition was found to lie at 2286.72 cm^{-1}. These measured values were within 0.1 cm^{-1} of measurements by Miescher,[13] who deduced the vibrational structure from electronic transitions of NO^*.

The concentration of NO^* was calculated using a least squares fit of the data to Eq. (8) assuming $\alpha_v = 4.3\times10^{-7}\ cm^3\ sec^{-1}\ (T_e/300)^{-0.37}$.[14] The relative population of the lower state involved in the absorption transition was then given by Eq. (6). Using this technique, the

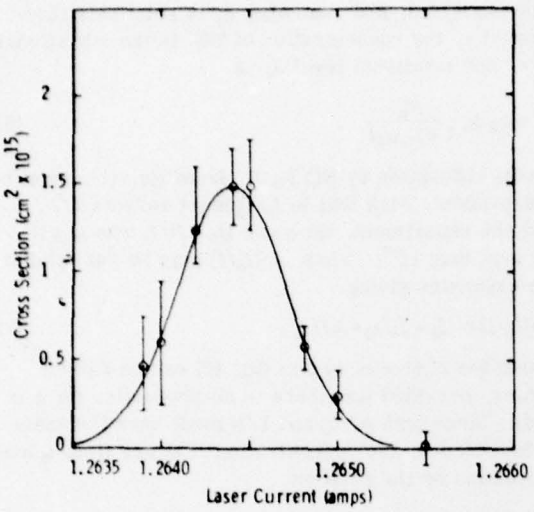

FIG. 5. Spectral absorption cross section of the $P5$ line of $v = 1$ to $v = 2$ level band of NO$^+$. Line center at 2291.63 ± 0.01 cm^{-1}, tuning ramp of 7 cm^{-1}/A.

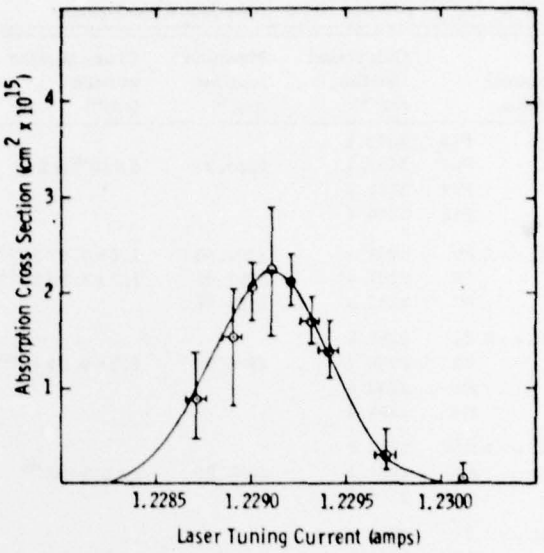

FIG. 6. Spectral absorption cross section of the $R2$ line in the $v = 2$ to $v = 3$ band. Tuning ramp equals 7 cm^{-1}/A. Line location at 2286.72 ± 0.01 cm^{-1}.

spectral absorption coefficient was obtained as a function of laser current from Eq. (1). The spectral absorption cross section for $P5$ line of the $v = 1$ to $v = 2$ and the $R2$ line of the $v = 2$ to $v = 3$ transitions are shown in Figs. 5 and 6, respectively. The laser current, plotted on the abscissa of these two figures, was fit to the tuning slope shown in Fig. 2 to obtain the linewidth. The tuning ramp was 7 cm^{-1} per A, giving an absorption half-width of 0.0056 cm^{-1}, approximately the Doppler width for NO$^+$ at 300 °K. A Doppler profile was thus fit through the experimental data to compute the integrated absorption coefficient. The absorption cross section was obtained by assuming that the relative population in the $v = 1$, $v = 2$, and $v = 3$ levels were 0.39, 0.22, and 0.08, respectively. The corresponding integrated absorption coefficients become $S_{12} = 236 \pm 20$ cm^{-2} atm^{-1} for the $P5(1-2)$ line and $S_{23} = 325 \pm 20$ cm^{-2} atm^{-1} for the $R2(2-3)$ line. Note that these absorption coefficients are taken with highly nonequilibrated vibrational temperatures. If we convert these absorption coefficients to their respective rates at thermodynamic equilibrium, their absorption coefficients become $S_{12} = 430 \pm 50$ and $S_{23} = 653 \pm 80$ cm^{-2} atm^{-1}, respectively. The larger error in the equilibrium calculation stems from the uncertainty in the relative populations of the $v = 1$, $v = 2$, and $v = 3$ levels of the photoionized NO.

Note that the ratio S_{23}/S_{12} is approximated 3/2. From these relative values, it may be assumed that NO$^+$ is a harmonic oscillator with a linear dipole moment derivative, in which case S_{01} may be extrapolated to give a value of $S_{01} \cong 215$ cm^{-2} atm^{-1}.

These integrated absorption coefficients may be converted into vibrational f numbers and Einstein A coefficients. The respective values for Einstein A coefficients of the $v = 1$ and $v = 2$ levels, together with the extrapolated $v = 0$ level, are listed in Table II. Also listed here are the corresponding values obtained by F. Billingsley from MCSCF calculations and obtained by H. H. Michels using CI calculations.

IV. MEASUREMENT OF THE NO$^+$ VIBRATIONAL EXCHANGE WITH N_2

The transfer rate of vibration from the $v = 1$ and $v = 2$ levels of NO$^+$ to N_2 was measured by observing absorption in the $P5$ and $R2$ absorption lines of these two vibrational levels, respectively. By using the absorption of infrared light as a monitor, the relative populations of the $v = 0$, $v = 1$, $v = 2$, and $v = 3$ levels were monitored as a function of N_2 pressure. Since the extinction of laser light is directly proportional to the population of the absorbing level, the time varying signal is a measure of vibrational transfer from NO$^+$. The disappearance of NO$^+(v)$ is from the following processes:

$NO^+(v) + e - N + O$ (R1), $\alpha = 4.3 \times 10^{-7} (T_e/300)^{-0.37}$ cm^3 sec^{-1} (Ref. 14),

$NO^+(v) + NO + NO - NO^+ \cdot NO + NO$ (R2), $k_2 = 5 \times 10^{-30}$ cm^6 sec^{-1} (Ref. 15)

$NO^+(v) + N_2 + N_2 - NO^+ \cdot N_2 + N_2$ (R3), $k_3 = 2 \times 10^{-31}$ cm^6 sec^{-1} (Ref. 15),

$NO^+(v) + NO - NO + NO^+(v-1)$ (R4), k_4 = this work,

and

$NO^+(v) + N_2 - NO^+(v-1) + N_2^+$ (R5), k_5 = this work.

TABLE II. Comparison of the measured NO* line strength with calculated values.

	S_{lu} ($cm^{-2}atm^{-1}$)		A_{ul} (sec^{-1})			f_{lu}	
	This work	SCF[4]	This work	SCF[4]	SCF[5]	This work	SCF[5]
$v=2-3$	653	176	95.8	26.2	73	2.7×10^{-6}	2.1×10^{-6}
$v=1-2$	430	176	63.4	26.2	51	1.8×10^{-6}	1.4×10^{-6}
$v=0-1$	215	88.9	31.5	13.6	26	9×10^{-6}	7×10^{-6}

The experimental technique for measuring the rate k_5 was to introduce N_2 into the absorption cell described in Sec. II at increasing pressures until the recombination rate α no longer dominates the disappearance of NO*(v). Since the absorption cross section of NO* is constant with time, the amount of absorption is proportional to the number density of NO* in the lower and upper states. The decrease in NO*(v) concentration with time is given by the sum of Reactions (R1) through (R5) minus the increase in NO*(v) concentration due to Reactions (R4) and (R5) on the ($v+1$) vibrational level. Reaction (R3) becomes important when N_2 within the test chamber exceeds 30 torr in this experiment. Note that in order to measure Reactions (R4) and (R5) for $v=1$, these reactions must be measured for $v=2$, etc. However, since the initial concentration of NO* in $v=4$ and above is negligible compared to $v=1$ and $v=2$, the quenching rate of $v=2$ and $v=1$ are not greatly effected by their quenching rates. Since the NO pressure was held constant at 1 torr, the effect of the association reaction (R2) was to increase the apparent rate of Reaction (R4) by the rate 1.6×10^{-13} cm^3sec^{-1}.

The quenching of NO*($v=3$) was measured by observing the decay of intensity of the $R11$ line of the $v=3$ to $v=4$ transition. The transient absorption signal by this line, proportional to the concentration of NO*($v=3$), can be represented as

$$[NO^*(v=3)](t)=\left[\phi_3 e^{-t/\tau_3}+\frac{\phi_4\tau_3(e^{-t/\tau_4}-e^{-t/\tau_3})}{\tau_4-\tau_3}\right]\left(\frac{n_0}{1+\alpha n_0 t}\right), \tag{9}$$

where n_0 is the initial concentration of NO*, ϕ_3 and ϕ_4 the initial fractions of [NO*] in the $v=3$ and $v=4$ levels corresponding to 0.08 and 0.02, respectively, and τ_3 and τ_4 are the quenching time constants for the $v=3$ and $v=4$ levels, respectively, given by

$$1/\tau_i=k_{4_i}[NO]+k_{5_i}[N_2]\,. \tag{10}$$

Since τ_4 was not measured, only a rough estimate of τ_3 can be obtained using the measured $[NO^*(v=3)](t)$. This was done by assuming a variety of values for τ_4. The fractions of NO* produced in the $v=3$ and $v=4$ levels were assumed to be 0.08 and 0.02, respectively. Thus, the quenching rate of the $v=4$ vibration could introduce an error of only 25% to the $v=3$ quenching.

Since no quenching rate was measured for the $v=4$ vibrational level, only a rough rate of

$$k_5(v=3)=2\pm1\times10^{-12}\ cm^3sec^{-1} \tag{11}$$

was obtained.

The time varying concentration of NO*($v=2$) is a function of this rate as well as the rate for quenching NO*($v=2$). This quenching rate is related to the time varying NO*($v=2$) concentration by

$$[NO^*(v=2)](t)=\left[\phi_2 e^{-t/\tau_2}+\frac{\phi_3\tau_2(e^{-t/\tau_3}-e^{-t/\tau_2})}{\tau_3-\tau_2}-\phi_4\frac{\tau_2\tau_3(e^{-t/\tau_4}-e^{-t/\tau_3})}{(\tau_3-\tau_2)(\tau_4-\tau_3)}+\frac{\phi_4\tau_2\tau_4(e^{-t/\tau_4}-e^{-t/\tau_2})}{(\tau_2-\tau_4)(\tau_4-\tau_3)}\right]\frac{n_0}{1+\alpha n_0 t}\,. \tag{12}$$

Note that the maximum effect of NO*($v=4$) on the concentration of NO*($v=2$) is less than ϕ_4/ϕ_2. Since this is less than a 10% effect, it may be neglected in the calculation of τ_2. The pressure of N_2 was varied while measuring the absorption of $v=2$ $R2$ line. The calculated time constant τ_2 from the time history of $[NO^*(v=2)](t)$ is plotted in Fig. 7 as a function of N_2 pressure.

The rate constants for k_4 and k_5 are obtained by fitting the time τ_2 from Eq. (10) with respective concentrations of N_2 and NO.

The partial pressure of NO within the test cell was 1 torr at all times to provide the photoionized NO*. By extrapolating to zero N_2 pressure, a quenching rate for NO was also inferred (see Fig. 7).

Using this technique, the vibrational quenching rate of NO*($v=2$) by N_2 was found to be

$$k_5=2.5\pm0.5\times10^{-12}\ cm^3sec^{-1}\,.$$

The quenching of NO*($v=2$) by NO was obtained by extrapolating the total quenching time plotted in Fig. 7 to zero N_2 pressure. Thus,

$$k_4(v=2)\,2.5\pm2\times10^{-13}\ cm^3sec^{-1}\,.$$

Using these rates obtained for $v=2$ together with measurements of the time rate of change to signal from the $P5$ line of the $v=1$ to $v=2$ transition, the quenching by N_2 and NO were obtained in a similar manner: Eq. (12) extended to $v=1$. The NO*($v=1$) quenching rate by N_2 becomes

$$k_5(v=1)=3\pm0.5\times10^{-12}\ cm^3sec^{-1}$$

and by NO is

$$k_4(v=1)\leq1.5\times10^{-13\pm0.5}\ cm^3sec^{-1}\,.$$

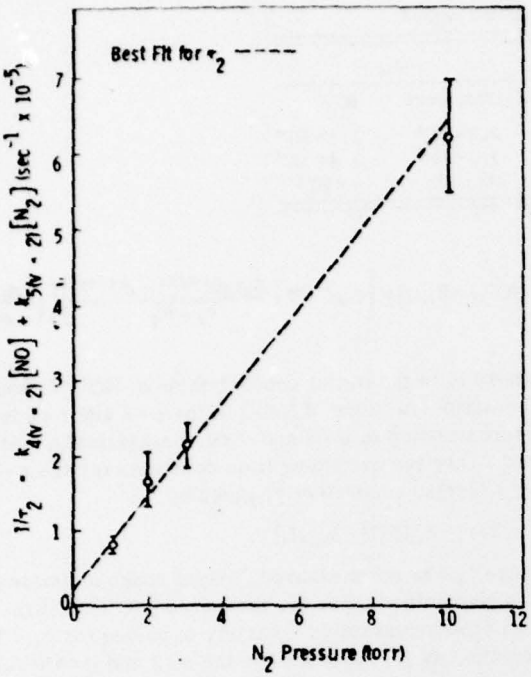

FIG. 7. Quenching of $v = 2$ NO$^+$ vibration by N_2 and NO. The pressure of NO was held to 1.00 torr at all times.

A measurement of vibrational transfer to $v = 0$ of NO$^+$ was attempted by monitoring the $P13$ line of $v = 0$ to $v = 1$. The initial vibrational population was inverted, i.e., there was more NO$^+(v = 1)$ than $(v = 0)$. Thus, negative absorption was monitored during the lamp pulse, which decayed to zero very quickly. This indicated either a more rapid recombination rate in the $v = 1$ level than in $v = 0$, or quenching of $v = 1$ by NO in the system. Upon introduction of N_2, it was hoped that absorption would be seen at late times, when NO$^+(v = 1)$ had been quenched to below the NO$^+(v = 0)$ concentration, but before dissociative recombination could take place. This effect was seen, but no quantitative information was available within the signal-to-noise ratio of the system.

V. DISCUSSION

The radiative lifetime of NO$^+$ has been calculated from measurements of absorption in the $v = 1$ and $v = 2$ levels. Since these rates are a function of the relative concentrations of NO$^+$ in the lower and upper states of the absorption, some uncertainty is introduced when relating the measured values to an absorption coefficient at thermal equilibrium. From these measurements, vibrational thermal equilibrium would occur only if the majority of NO$^+$ vibrational excitation was quenched by N_2 before recombination could take place.

The ratio of absorption coefficient between $v = 2$ to $v = 3$ and $v = 1$ to $v = 2$ transitions appear to follow the rules of a simple diatomic molecule with a linear dipole moment derivative around the equilibrium intermolecular separation, i.e., $S_{1a} \sim (v+1)S_{01}$, where v is the vibrational level of the lower state. Using this scaling, the integrated absorption coefficient of the $v = 0$ vibrational level would be 215 cm^{-2} atm^{-1} as listed in Table II. This value is not too different from the value which Billingsley[4] would obtain using a slightly different dipole moment derivative in place of his multiconfiguration SCF calculated result. Using his single configuration Hartree–Fock calculations, Billingsley obtains an integrated absorption coefficient of 251 cm^{-2} atm^{-1} compared to his published 88.9 cm^{-2} sec^{-1}. This value would be within 20% of our measured value. Similarly, our number differs from Michels' calculated number by 25%, well within the error bars of either our measurement, or his calculations.

Our value for the integrated absorption coefficient of NO$^+$ in the $v = 2$ to $v = 3$ transition is not in disagreement with the Stair and Gauvin[3] observations, as their assumptions of thermodynamic equilibrium between NO$^+$ and CO in order to arrive at their integrated intensities allow for errors as large as a factor of 3. Since the NO$^+$ produced in the upper atmosphere is by no means in thermal equilibrium, and with the rapid dissociative recombination of NO$^+$, thermal equilibrium between NO$^+$ and CO would indeed be fortuitous.

Other sources of error in the measurement of the NO$^+$ f number are in the uncertainty within the extent of the photoionization region, which could introduce a ± 5% error, and in the slight detuning of the diode laser during lamp discharge, which would change the NO$^+$ line location by ± 0.005 cm^{-1}. These sources of error are much less important, however, than the uncertainty in the number density of NO$^+$ (v, J). Finally, the NO γ, δ, and ϵ bands excited by the uv flash lamps may all have vibration rotation lines within the NO$^+$ vibrational frequency range. These electronic bands have radiative lifetimes on the order of 0.4 μsec, however, so their absorption of infrared radiation quickly disappears after the flash lamp turns off. The absorption of laser light by these bands during the lamp flash gave what at first appeared to be a very long spectral tail in the NO$^+$ absorption, which could have been prevented by using a long wavelength cut off filter in front of each flash lamp. As it turned out, because of the very short lifetime of these states, their effect was to provide a better base level from which to determine lamp shut off.

The measurement of NO$^+(v)$ transfer to N_2 was somewhat more accurate than that of the NO$^+$ vibrational lifetime, since the absolute number density of NO$^+(v)$ was not necessary for this determination. While the integrated absorption of excited NO$^+(v)$ scaled approximately as $(v+1)$, no such simple scaling was available on NO$^+(v)$ transfer to N_2. This transfer rate was seen to decrease slightly for higher vibrational levels of NO$^+$, rather than increasing. If this trend holds for vibrational levels higher than 3, it would be expected that NO$^+$ formed in the high vibrational levels would contribute most of the radiation in the upper atmosphere. Since only transfer from $v = 1$ and $v = 2$ levels were measured in detail, however, this is a premature conclusion.

While no previous measurements have been made on NO$^+(v)$ quenching by N_2, various estimates have been made based on the observations of auroral activity.[17]

From the lack of detection of $NO^+(v)$ in the upper atmosphere, quenching rate estimates of as high as 10^{-9} cm^{-3} sec^{-1} have been proposed. Due to the extremely good overlap of NO^+ with CO_2, however, the lack of any detectable NO^+ may be due to the fact that the signal is buried within the very large CO_2 signature. It is interesting to note that quenching of NO^+ by N_2 is on the order of 10 times more efficient than the transfer of $CO_2(\nu_3)$ to N_2. This could easily be accounted for by the ionic nature of NO^+ as well as its dipole moment. This higher quenching rate, together with the factor of 10^3 lower NO^+ concentration than CO_2 concentration, even during an IBC class II aurora,[18] would mean NO^+ emission is 10^4 weaker than $CO_2(\nu_3)$ in an auroral event.

In conclusion, both the $NO^+(v)$ radiative lifetime and the transfer of vibration to N_2 have been measured in this experiment. While both these measurements were the first to be performed on the NO^+ ion, they agree at least qualitatively to values inferred from upper atmospheric studies. In order to obtain a better picture of the NO^+ emission during electron disturbances in the upper atmosphere, both the degree of vibrational excitation during NO^+ formation and the transfer of vibration to O and O_2 must also be measured.

ACKNOWLEDGMENTS

The author would like to thank Drs. Morton Camac and Lawrence Bernstein for the many helpful suggestions during the various phases of this work, and Mr. Robert Brown for his invaluable assistance in the laboratory.

[1]J. Ulwick, ICECAP 1975 Data, presented at DNA HAES Meeting (June 1977).
[2]J. Kumer, "Analysis of 4.3 μ ICECAP Data," Report AFCRL-TR-740334 (July 1974).
[3]A. T. Stair and H. P. Gauvin, *Aurora and Airglow*, edited by B. M. McCormac (Reinhold, New York, 1967).
[4]F. P. Billingsley, II, Chem. Phys. Lett. **23**, 160 (1973).
[5]H. H. Michels "Air Molecular Computation Study," Report AFGL-TR-77 0032 (1977).
[6]T. U. White, J. Opt. Soc. Am **32**, 285 (1942).
[7]T. Lyman, Science **64**, 89 (1926).
[8]J. F. Holzrichter and J. L. Emmett, Appl. Opt. **8**, 1459 (1969).
[9]K. Tanaka, K. Honma, I. Loyano, and I. Tanaka, J. Chem. Phys. **60**, 3347 (1974).
[10]P. C. Killgoar, Jr., G. E. Leroi, J. Berkowitz, and W. A. Chupka, J. Chem. Phys. **58**, 803 (1973).
[11]K. Watanabe, F. M. Matsunaga, and H. Sakai, Appl. Opt. **6**, 391 (1967).
[12]R. Oberly, K. N. Rao, Y. H. Hahn, and T. K. McCubbin, Jr., J. Mol. Spectrosc. **25**, 138 (1968).
[13]E. Miescher, Helv. Phys. Acta **29**, 135 (1956).
[14]C. M. Huang, M. A. Biondi, and R. Johnsen, Phys. Rev. A **11**, 901 (1975).
[15]W. C. Lineberger and L. J. Puckett, Phys. Rev. **186**, 116 (1969).
[16]R. Johnsen, C. M. Huang, and M. A. Biondi, J. Chem. Phys. **63**, 3374 (1975).
[17]D. H. Archer (private communication).
[18]R. S. Narcisi, C. Sherman, L. E. Wlodyka, and J. C. Ulwick, J. Geophys. Res. **79**, 2843 (1974).

DNA Distribution List

Department of Defense

Director
Defense Advanced Research Projects Agency
1400 Wilson Boulevard
Arlington, VA 22209

1 cy ATTN: TIO
1 cy ATTN: STO
1 cy ATTN: NRMO

Director
Defense Communications Agency
8th Street and Courthouse Road
Arlington, VA 22204

3 cys ATTN: MEECN Office

Defense Documentation Center
Cameron Station
Alexandria, VA 22314

12 cys ATTN: TC

Director
Defense Nuclear Agency
Washington, D. C. 20305

1 cy ATTN: STTL
1 cy ATTN: DDST
3 cys ATTN: RAAE
1 cy ATTN: RAEV

Department of Defense (Continued)

Joint Chiefs of Staff
Department of Defense
Washington, D. C. 20301

1 cy ATTN: J-6

Director
National Security Agency
Fort George G. Meade, MD 20755

2 cys ATTN: Technical Library

Under Secretary of Defense (Research and Engineering)
Department of Defense
Washington, D. C. 20301

2 cys ATTN: DDS&SS

Department of Commerce

U. S. Department of Commerce
Office of Telecommunications
Institute for Telecommunication Sciences
National Telecommunications and Information Administration
Boulder, CO 80303

2 cys ATTN: W. F. Utlaut

Department of the Army

Commander/Director
Atmospheric Sciences Laboratory
U. S. Army Electronics Command
White Sands Missile Range, NM 88002

1 cy ATTN: DRSEL-BL-SY-S
F. E. Niles

Director
U. S. Army Ballistic Research Laboratories
Aberdeen Proving Grounds, MD 21005

1 cy ATTN: George E. Keller

Commander
U. S. Army Foreign Sciences and Technology Center
220 7th Street, N.E.
Charlottesville, VA 22901

1 cy ATTN: Robert Jones

Department of the Navy

Chief of Naval Operations
Department of the Navy
Washington, D.C. 20350

1 cy ATTN: NOP 985
1 cy ATTN: NOP 094H

Department of the Navy (Continued)

Chief of Naval Research
Department of the Navy
800 North Quincy Street
Arlington, VA 22217

1 cy ATTN: Code 465, R. G. Joiner
1 cy ATTN: Code 427, H. Mullaney

Commander
Naval Electronic Systems Command
Department of the Navy
Washington, D.C. 20360

1 cy ATTN: PME-117
1 cy ATTN: PME-117T
1 cy ATTN: PME-117-21
1 cy ATTN: PME-117-21A
1 cy ATTN: PME-117-22

Director
Naval Ocean Systems Center
Electromagnetic Propagation Division
271 Catalina Boulevard
San Diego, CA 92152

1 cy ATTN: Code 2200, W.F. Moler
1 cy ATTN: Code 2200, Ilan Rothmuller
1 cy ATTN: Code 2200, John Bickel

Director
Naval Research Laboratory
4555 Overlook Avenue, S.W.
Washington, D.C. 20375

1 cy ATTN: Code 7700, Timothy P. Coffey
1 cy ATTN: Code 7709, Wahab Ali
2 cys ATTN: Code 7750, John Davis
1 cy ATTN: Code 2627

Commander
Naval Surface Weapons Center (White Oak)
Silver Spring, MD 20910

1 cy ATTN: Technical Library

Office of Naval Research Branch Office
1030 East Green Street
Pasadena, CA 91106

1 cy

Department of the Air Force

Commander
Air Force Geophysical Laboratory, AFSC
L. G. Hanscom Air Force Base, MA 01731

1 cy ATTN: OPR, James Ulwick
1 cy ATTN: LKB, W. Swider
1 cy ATTN: LKB, K. Champion

Director
Air Force Technical Applications Center
Patrick Air Force Base, FL 32920

1 cy ATTN: TD
1 cy ATTN: HQ 1035th TCHOG/TFS

Department of Defense Contractors

General Electric Company
TEMPO - Center for Advanced Studies
816 State Street
Santa Barbara, CA 93102

1 cy ATTN: Warren S. Knapp
1 cy ATTN: DASIAC

Lockheed Missiles and Space Company
3251 Hanover Street
Palo Alto, CA 94304

1 cy ATTN: J. B. Reagan
1 cy ATTN: W. Imhof
1 cy ATTN: Martin Walt

Mission Research Corporation
735 State Street
Santa Barbara, CA 93101

1 cy ATTN: M. Scheibe
1 cy ATTN: D. Sowle

Pacific-Sierra Research Corporation
1456 Cloverfield Boulevard
Santa Monica, CA 90404

1 cy ATTN: E. C. Field

Pennsylvania State University
Ionospheric Research Laboratory
College of Engineering
318 Electrical Engineering - East Wing
University Park, PA 16802

1 cy ATTN: John S. Nisbet
1 cy ATTN: Les Hale
1 cy ATTN: A. J. Ferraro
1 cy ATTN: H. S. Lee

R&D Associates
4640 Admiralty Way
Marina Del Rey, CA 90291

1 cy ATTN: R. Lelevier
1 cy ATTN: F. Gilmore
1 cy ATTN: R. Turco

The Rand Corporation
1700 Main Street
Santa Monica, CA 90406

1 cy ATTN: Cullen Crain

Professor Chalmers F. Sechrist
155 Electrical Engineering Building
University of Illinois
Urbana, IL 61801

1 cy ATTN: C. Sechrist

Stanford Research Institute
333 Ravenswood Avenue
Menlo Park, CA 94025

1 cy ATTN: Allen M. Peterson
1 cy ATTN: Ray L. Leadabrand

University of Pittsburgh
Dept. of Physics & Astronomy
Pittsburgh, PA. 15260

1 cy ATTN: M.A.Biondi
1 cy ATTN: F.Kaufman
1 cy ATTN: W.Fite

General Electric CO. , Space Division, VFSC
Goddard Blvd., King of Prussia
P.O.Box 8555
Philadelphia, PA 19101

1 cy ATTN: M.H.Bortner
1 cy ATTN: T.Baurer

National Oceanic & Atmospheric Admin.
Environmental Research Laboratories
Dept. of Commerce
Boulder, CO 80302

1 cy ATTN: E.E.Ferguson
1 cy ATTN: F.Fehsenfeld